

# HNCO + $h\nu(193.3 \text{ nm}) \rightarrow \text{H} + \text{NCO}$ : Center-of-Mass Translational Energy Distribution, Reaction Dynamics, and $D_0(\text{H}-\text{NCO})^\dagger$

Jingsong Zhang, Michael Dulligan, and Curt Wittig\*

Department of Chemistry, University of Southern California, Los Angeles, California 90089-0482

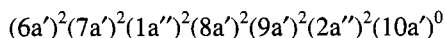
Received: October 17, 1994<sup>⊗</sup>

The  $\text{H} + \text{NCO}(\text{X}^2\Pi)$  channel in the 193.3-nm photodissociation of HNCO has been examined by using high- $n$  Rydberg hydrogen atom time-of-flight (HRTOF) spectroscopy, and the center-of-mass (cm) translational energy distribution has been obtained. The cm translational energy distribution peaks near the maximum available energy and shows considerable structure corresponding to NCO vibrational excitation. This is attributed to geometric changes in going from HNCO to the electronically excited potential surface then to products. Specifically, a strongly bent N–C–O angle in excited HNCO accounts for the long NCO bending progression that is observed. A strongly anisotropic product angular distribution was observed, in agreement with an  $^1\text{A}''$  excited state and rapid dissociation via a repulsive surface.  $D_0(\text{H}-\text{NCO})$  is found to be  $110.1 \pm 0.5 \text{ kcal mol}^{-1}$ , in agreement with recent experimental and theoretical values.

## I. Introduction

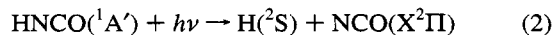
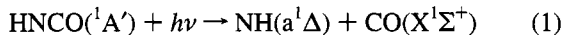
Isocyanic acid (HNCO) is an important species in the combustion of nitrogenous fuels in the atmosphere.<sup>1–5</sup> For example, it is believed to play a significant role in the rapid reduction of nitrogen oxides (RAPRENO<sub>x</sub>), which is important in NO<sub>x</sub> emission control.<sup>1–2</sup> It is also a convenient photolytic source of NCO and NH radicals.

HNCO is a 16-valence-electron molecule having  $C_s$  symmetry and the ground-state electronic configuration



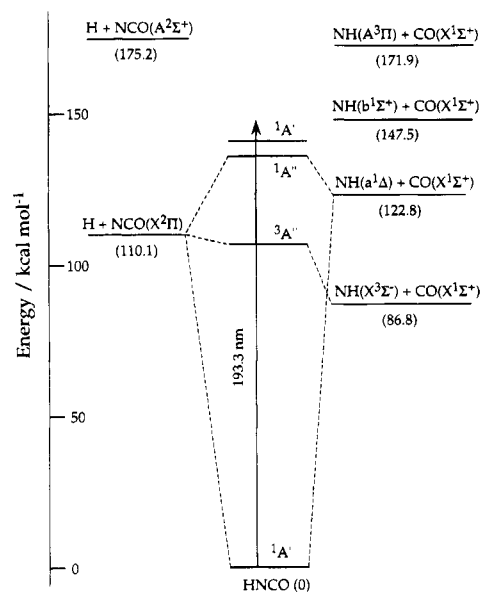
Its 180–280-nm absorption spectrum is broad and continuous with weak superimposed vibrational bands above 220 nm. It has been analyzed by Dixon and Kirby<sup>6</sup> and by Rabalais et al.<sup>7,8</sup> and assigned to an  $^1\text{A}'' \leftarrow ^1\text{A}'$  transition to the lowest excited singlet:  $(2a'')^1(10a')^1 \leftarrow (2a'')^2$ . The coarse rotational structure at long wavelengths enabled Dixon and Kirby to show that the excited state was bent with an N–C–O angle of about  $120^\circ$ . This differs considerably from the ground state, whose N–C–O angle is near  $180^\circ$ .<sup>9–11</sup> HNCO has also been examined in the vacuum ultraviolet (VUV).<sup>12,13</sup>

Figure 1 shows an energy diagram relevant to the present work. There have been many photochemical studies and two low-energy, spin-allowed channels have been observed.<sup>14–23</sup>



Bradley et al. showed that with decreasing wavelength the participation of channel (1) increases relative to that of channel (2),<sup>16</sup> while more recent studies demonstrated that channel (2) is minor at 193.3 nm.<sup>19,20</sup> Specifically, an upper bound of 0.10 for the NCO/NH branching ratio was reported by Spiglanin et al.,<sup>19</sup> while Yi and Bersohn reported an H atom quantum yield of 0.05.<sup>20</sup>

Channel (1) has been studied extensively at convenient ultraviolet wavelengths.<sup>17–19,21–23</sup> NH is produced in the lowest



**Figure 1.** Energy level and state correlation diagram of the HNCO system. Energies are from refs 7, 28, 35, and 47 and this study.

singlet ( $a^1\Delta$ ) instead of the  $\text{X}^3\Sigma^-$  ground state, since the lowest spin-allowed channel is  $\text{NH}(a^1\Delta) + \text{CO}(\text{X}^1\Sigma)$ . Drozdowski et al. measured the NH state distribution by using laser-induced fluorescence (LIF) following 193.3-nm photodissociation.<sup>17</sup> They found that  $\text{NH}(a^1\Delta)$  was formed primarily in  $v = 0$ , with rotational excitation accounting for about 8% of the available energy;  $\text{NH}(\text{X}^3\Sigma^-)$  was not observed. Fujimoto et al. probed  $\text{CO}(v)$  following 193.3-nm photolysis<sup>18</sup> and levels up to  $v = 4$  were observed. The average CO vibrational energy was about 15% of the available energy, and the distribution could be fit by using a statistical model and assuming that NH was in the  $a^1\Delta$  state.<sup>18</sup> Spiglanin et al. studied channel (1) at various wavelengths and obtained information concerning its dynamics.<sup>19,21,22</sup> Nascent NH and CO state distributions were obtained by using LIF<sup>19,21b</sup> and multiphoton ionization,<sup>19,21a</sup> respectively, and CO translational energies were measured by using multiphoton ionization translational spectroscopy.<sup>22</sup> The NH and CO state distributions at 230 and 193.3 nm could not be fitted by using phase space theory (PST). Instead, they were rationalized by using an impulsive model, with dissociation

<sup>†</sup> Research supported by the Department of Energy under Contract DE-FG03-85ER13363.

<sup>⊗</sup> Abstract published in *Advance ACS Abstracts*, May 1, 1995.

**TABLE 1: Fractional Energy Release in the UV Photodissociation of HNCO**

HNCO( $^1A'$ ) + $h\nu \rightarrow$ NH( $a^1\Delta$ ) + CO( $X^1\Sigma^+$ )					
$\lambda$ , nm	$\langle f_{\text{rot}} \rangle_{\text{NH}}$	$\langle f_{\text{vib}} \rangle_{\text{NH}}$	$\langle f_{\text{rot}} \rangle_{\text{CO}}$	$\langle f_{\text{vib}} \rangle_{\text{CO}}$	$\langle f_{\text{trans}} \rangle$
193.3	0.08–0.11 <sup>a,c</sup>	0.074 <sup>d</sup>	0.20 <sup>b</sup>	0.15 <sup>e</sup>	0.47–0.50
230	0.04 <sup>c</sup>		0.18 <sup>b</sup>		
HNCO( $^1A'$ ) + $h\nu \rightarrow$ H( $^2S$ ) + NCO( $X^2\Pi$ )					
$\lambda$ , nm	$\langle f_{\text{trans}} \rangle$	$\langle f_{\text{int}} \rangle_{\text{NCO}}$			
193.3	0.32 <sup>f</sup>	0.68 <sup>f</sup>			
193.3	0.70 <sup>g</sup>	0.30 <sup>g</sup> ( $f_{\text{vib}} \approx 0.26$ , $f_{\text{rot}} \approx 0.04$ )			

<sup>a</sup> Reference 17. <sup>b</sup> Reference 21a. <sup>c</sup> Reference 21b. <sup>d</sup> Reference 23. <sup>e</sup> Reference 18. <sup>f</sup> Reference 20. <sup>g</sup> This study.

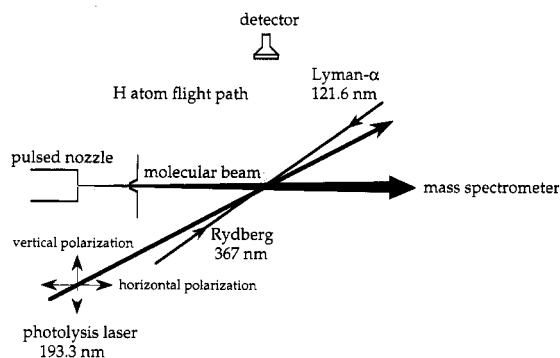
occurring on an excited-state potential energy surface (PES) having a bent N–C–O configuration.<sup>19,21,22</sup> Recently, Bohn and Stuhl measured the NH( $a^1\Delta$ ) vibrational distribution with great care following 193.3-nm excitation.<sup>23</sup> The average NH vibrational energy was shown to be about 7% of the available energy, with a monotonically decreasing population from  $v = 0$  to 2. This is consistent with direct dissociation on a repulsive PES, which channels a large fraction of the excess energy into cm translation.<sup>23</sup> Energy partitioning for channel (1) at 193.3 nm is summarized in Table 1.

Channel (2) has not been studied as thoroughly. Drozdowski et al. were unable to detect NCO via LIF,<sup>17</sup> while Spiglanin et al. did detect NCO via LIF, though little dynamical information was obtained.<sup>20</sup> Yi and Bersohn studied this channel at 193.3 nm by detecting H atoms via LIF.<sup>19</sup> Average translational energies were determined from Doppler broadened spectra, and the average cm translational energy was found to be 32% of the available energy, assuming an isotropic product angular distribution. From their results, they infer that the HNC and NCO angles are both strongly bent in the excited state.

Despite the importance of HNCO and NCO, there have been questions about their thermochemistries. The H–NCO dissociation energy was first determined by Okabe, who studied the VUV photodissociation.<sup>12</sup> Several electronically excited species were observed by fluorescence following photoexcitation. By measuring the appearance threshold for NCO( $A^2\Sigma$ ) and combining it with the  $A^2\Sigma$  electronic energy, an upper bound of  $113.0 \pm 0.2$  kcal mol<sup>-1</sup> was established.<sup>12</sup> Uno et al. studied VUV photodissociation with synchrotron radiation and reported an upper bound of 111 kcal mol<sup>-1</sup>.<sup>13</sup> Electron impact dissociation was investigated by Tokue and Ito.<sup>24</sup> The NCO-( $A^2\Sigma$ ) onset was measured, yielding an upper bound of  $126 \pm 14$  kcal mol<sup>-1</sup>, and they suggested that this large value might be due to the  $A^2\Sigma$  vibration–rotation energy acquired in the dissociation process. The studies reported in refs 13, 17, and 24 do not yield well-defined thermodynamic quantities directly, since they rely on appearance thresholds and detection sensitivity. We use the symbol  $D(\text{H–NCO})$  to denote these quantities.

Recently, Ruscic and Berkowitz carried out a photoionization mass spectrometric study of HNCO under well-characterized conditions.<sup>25</sup> Both the appearance potential (NCO<sup>+</sup>/HNCO) and ionization potential of NCO were measured, and the difference yielded  $D_0(\text{H–NCO}) \leq 110.1 \pm 0.3$  kcal mol<sup>-1</sup>.

There have also been several theoretical studies of  $D_0(\text{H–NCO})$ . Yokoyama et al. obtained 107 kcal mol<sup>-1</sup> by using the MRD-CI method,<sup>26</sup> while East, Johnson, and Allen used various ab initio methods to obtain  $112 \pm 2$  kcal mol<sup>-1</sup>.<sup>27</sup> In further work,<sup>28</sup> East and Allen calculated the NCO heat of formation. Five independent reactions were examined to establish a consistent value, two of which involve HNCO, i.e., HNCO  $\rightarrow$  H + NCO( $^2\Pi$ ) and HNCO  $\rightarrow$  H<sup>+</sup> + NCO<sup>-</sup>. In the first,  $D_0(\text{H–NCO})$  was found to be 110.4 kcal mol<sup>-1</sup>. In the second,

**Figure 2.** Schematics of the HRTOF apparatus.

the calculated heat of reaction was combined with the hydrogen ionization potential and the NCO electron affinity, yielding  $D_0(\text{H–NCO}) = 110.5$  kcal mol<sup>-1</sup>. An uncertainty of approximately 1 kcal mol<sup>-1</sup> was stated. Reliability was supported by the fact that the NCO heat of formation estimated by using the  $D_0(\text{H–NCO})$  values from the above two reactions agreed with that calculated from the other three reactions, which did not involve HNCO.

In Okabe's study, the NH( $c^1\Pi$ ) appearance threshold indicated an HN–CO dissociation energy  $D(\text{HN–CO}) \leq 78 \pm 2$  kcal mol<sup>-1</sup>.<sup>12</sup> From this and the known heats of formation of NH and CO, the heat of formation of HNCO was found to be  $-23 \pm 3$  kcal mol<sup>-1</sup> from the relationship

$$\Delta H_f^0(\text{HNCO}) = \Delta H_f^0(\text{NH}) + \Delta H_f^0(\text{CO}) - D(\text{HN–CO}) \quad (3)$$

An NCO heat of formation of  $36.9 \pm 3.5$  kcal mol<sup>-1</sup> was obtained by using  $D(\text{H–NCO}) = 113.0$  kcal mol<sup>-1</sup> with the relationship

$$\Delta H_f^0(\text{NCO}) = D(\text{H–NCO}) - \Delta H_f^0(\text{H}) + \Delta H_f^0(\text{HNCO}) \quad (4)$$

Spiglanin et al. obtained  $D(\text{HN–CO}) = 82.9$  kcal mol<sup>-1</sup> by measuring the NH( $a^1\Delta$ ) appearance threshold and NH and CO internal energies following HNCO photolysis near the dissociation threshold.<sup>19</sup>  $\Delta H_{f,298}^0(\text{HNCO})$  from eq 3 was  $-24.9_{-2.8}^{+0.7}$  kcal mol<sup>-1</sup>. Using Okabe's value of  $D(\text{H–NCO})$ , the NCO heat of formation is  $36.1_{-2.8}^{+0.7}$  kcal mol<sup>-1</sup>. Cyr et al. studied NCO dissociation and by determining the threshold of the spin-allowed N( $^2D$ ) + CO( $^1\Sigma^+$ ) channel obtained  $\Delta H_{f,0}^0(\text{NCO}) = 30.5 \pm 1$  kcal mol<sup>-1</sup>,<sup>29</sup> which is several kcal mol<sup>-1</sup> lower than the previously accepted value. There have been several theoretical studies of  $\Delta H_{f,0}^0(\text{NCO})$ . Lin et al. obtained  $32.1 \pm 4.8$  kcal mol<sup>-1</sup> by using BAC/MP4,<sup>30</sup> while East et al. used various electronic structure methods to obtain  $31.9 \pm 0.5$  kcal mol<sup>-1</sup>.<sup>28</sup> Clearly,  $D_0(\text{H–NCO})$  is needed to compare the NCO heats of formation from the Spiglanin et al. and Cyr et al. studies.

A direct, accurate determination of  $D_0(\text{H–NCO})$  will help to establish the thermochemistry of both the HNCO molecule and the NCO radical.

## II. Experimental Section

High- $n$  Rydberg time-of-flight (HRTOF) spectroscopy was used in this study (see Figure 2).<sup>31–33</sup> Only a brief description is given here, as it has been described in detail previously. A pulsed molecular beam was produced by expanding 3–4% HNCO in He at total pressures of  $\sim 700$  Torr. Mixtures were expanded into the source chamber through a 0.75-mm-diameter pulsed nozzle (General Valve, Series-9) operating at 10 Hz with a 500- $\mu$ s pulse width. The molecular beam was differentially pumped and collimated by a 1-mm-diameter skimmer 2 cm from the nozzle. Five centimeters further downstream, the molecular

beam was crossed with the photolysis radiation, i.e., a portion of the output from an ArF excimer laser (Questek 2820). This beam was focused with a 60-cm *f.l.* quartz lens and passed through an iris in front of the chamber. Typically 4–30 mJ of 193.3-nm radiation entered the vacuum chamber. This radiation could be polarized with an eight-plate stack of quartz slides placed at the Brewster angle, resulting in approximately 90% polarization. Hydrogen atoms produced from photodissociation were excited by VUV radiation tuned to line center of the Lyman- $\alpha$  transition at 121.6 nm. This radiation was generated by tripling the 364.7-nm output from an excimer-pumped dye laser (Lambda-Physik 3002) in Kr<sup>34</sup> and was focused into the interaction region by a MgF<sub>2</sub> lens. Another excimer pumped dye laser (Lambda-Physik 2001) excited the H atoms from the 2<sup>2</sup>P level to a high-*n* Rydberg level ( $n = 40$ – $90$ ). Some H<sup>+</sup> ions were generated from photoionization of hydrogen by the simultaneous presence of 364.7- and 121.6-nm radiations. A small negative potential was applied below the interaction region to prevent positive ions from reaching the detector. The high-*n* Rydberg states are radiatively metastable and stay highly excited for many tens of microseconds while they drift with their nascent velocities to the chevron microchannel plate (MCP) detector (Galileo Electro-Optics). Upon arrival at the detector, the excited atoms are efficiently field-ionized as they pass a wire mesh; they are then detected as ions. TOF spectra were recorded by using a transient digitizer (Transiac DSP 2001) and were averaged and stored on a computer. The flight distance was calibrated by photodissociating HBr, since its bond energy<sup>35</sup> and the Br spin-orbit splitting<sup>36</sup> are known with precision. The nominal flight length was 34.2 cm. The sampling interval of the transient digitizer was 20 ns and typically 1200–2000 channels around the region of interest were recorded; spectra usually represent  $(2$ – $6) \times 10^4$  laser firings.

HNCO was prepared by heating potassium cyanate (KOCN) in excess stearic acid under vacuum for  $\sim 4$  h by using a mineral oil bath at  $\sim 90$  °C.<sup>17,18,37</sup> Volatile substances were collected in a liquid nitrogen trap at  $-196$  °C. Impurities, mainly CO<sub>2</sub> and water, were removed by trap-to-trap distillations at  $-60$  and  $-120$  °C. Purified samples were stored at  $-78$  °C (acetone/dry ice) to prevent polymerization; long-term storage is possible at this temperature. Purity was verified by infrared,<sup>10</sup> UV,<sup>6</sup> and mass spectroscopies.<sup>15a,38</sup> HNCO vapor pressure versus temperature is available in the literature.<sup>39</sup> Molecular beams were produced by passing He through the HNCO bubbler cooled by low-temperature baths to achieve various HNCO concentrations. The molecular beams were monitored with a quadrupole mass spectrometer (UTI-100C). It was important to keep the HNCO sample below  $-30$  °C ( $\approx 52$  Torr vapor pressure) due to significant polymerization above this temperature.<sup>6,10,37</sup>

### III. Results and Analysis

#### A. Translational Energy Distribution and $D_0(\text{H-NCO})$ .

To correct for background, spectra were taken with the molecular beam alternately on and off with other experimental conditions the same; background was then subtracted. One such hydrogen TOF spectrum is shown in Figure 3. The more relevant distribution is for the cm translational energy, which is given by

$$E_{\text{cm}} = \left(1 + \frac{m_{\text{H}}}{m_{\text{NCO}}}\right)E_{\text{H}} + \frac{m_{\text{H}}}{m_{\text{NCO}}}E_{\text{HNCO}} \quad (5)$$

where  $E_{\text{H}}$  and  $E_{\text{HNCO}}$  are laboratory translational energies of H atoms and HNCO, respectively. Clearly the first term dominates. The second term is due to HNCO traveling with the molecular beam velocity and is the correction due to the motion

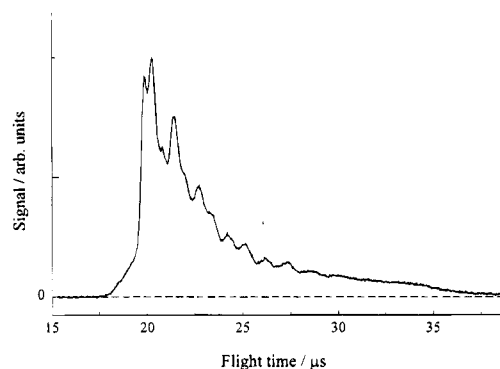


**Figure 3.** TOF data from photodissociation of HNCO at 193.3 nm (28 mJ).

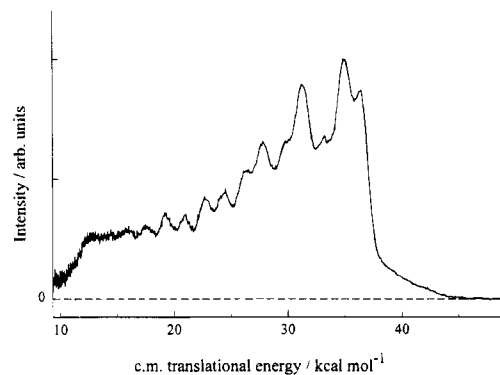


**Figure 4.** Center-of-mass translational energy distribution for photodissociation of HNCO; conditions as per Figure 3.

of the cm system. It is small ( $\leq 0.3$  kcal mol<sup>-1</sup>) because the H atom speed is much larger than the speed of the molecular beam. Transforming probability distribution from time to energy gives

$$S(E_{\text{cm}}) \sim s(t)t^3 \quad (6)$$

where  $s(t)$  is the arrival time spectrum. The spectrum  $S(E_{\text{cm}})$  is shown in Figure 4. An upper limit to  $D_0(\text{H-NCO})$  can be obtained from the expression

$$h\nu + E_{\text{int}}(\text{HNCO}) = D_0(\text{H-NCO}) + E_{\text{cm}} + E_{\text{int}}(\text{NCO}) \quad (7)$$

Since HNCO is internally cold (i.e., its rotational energy is  $\leq 0.1$  kcal mol<sup>-1</sup> and its vibrational energy before supersonic expansion is  $\sim 0.2$  kcal mol<sup>-1</sup>),  $E_{\text{int}}(\text{HNCO})$  is negligible. The error introduced by its neglect is lessened by also neglecting the second term in eq 5, since they contribute in opposite directions. Thus, eq 7 becomes:

$$h\nu = D_0(\text{H-NCO}) + \left(1 + \frac{m_{\text{H}}}{m_{\text{NCO}}}\right)E_{\text{H}} + E_{\text{int}}(\text{NCO}) \quad (8)$$

If the highest translational energy corresponds to the NCO ground state,  $D_0(\text{H-NCO})$  achieves its upper limit, which is given by the inequality

$$D_0(\text{H-NCO}) \leq h\nu - \left(1 + \frac{m_{\text{H}}}{m_{\text{NCO}}}\right)E_{\text{H}}^{\text{max}} \quad (9)$$

Care is essential when identifying the maximum translational energy. For example, Figure 3 shows that the fastest portion of the TOF spectrum has a slope that differs significantly from that of the sharply rising peak, suggesting possible contributions from one or more competing factors, e.g., multiphoton processes, hot-band dissociation, and clusters.

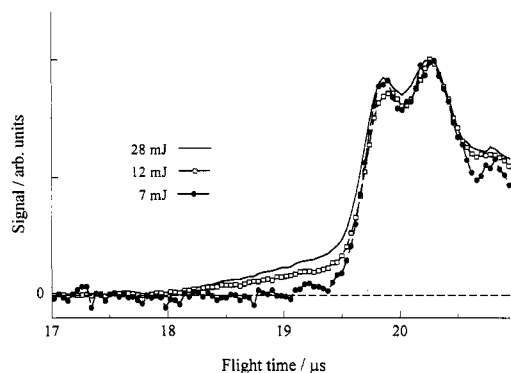


Figure 5. TOF spectra for different 193.3-nm laser fluences.

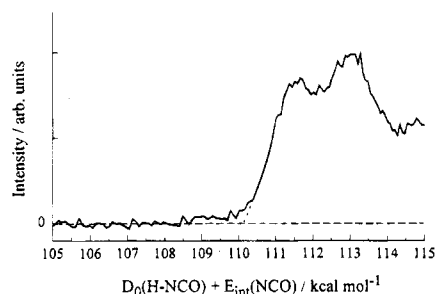


Figure 6. Relative intensity vs  $D_0(\text{H-NCO}) + E_{\text{int}}(\text{NCO})$ . The onset corresponds the minimum of  $E_{\text{int}}(\text{NCO})$  and thus the upper limit for  $D_0(\text{H-NCO})$ . See text for details.

To determine the extent of hot-band contributions, expansion conditions were varied drastically, i.e., 5, 23, and 55 Torr of HNCO in He with stagnation pressures of 100, 700, and 2000 Torr. The resulting HNCO concentrations varied from 0.2% to 55%. Spectra recorded under these conditions showed that varying the beam expansion conditions affected the cooling of HNCO and therefore the resolution of the spectra. However, there were only small variations in the shapes and relative intensities of the fast leading edge. Furthermore, the amount of HNCO vibrational energy is small ( $\sim 0.2 \text{ kcal mol}^{-1}$  at 298 K). Nonetheless, the leading edge extends for several kilocalories per mole. Thus, it is reasonable to assume that there is no significant contribution from vibrationally excited HNCO.

The fluence dependence was examined by carrying out experiments with photolysis energies of 28, 12, and 7 mJ. As shown in Figure 5, the relative intensities of the leading edges varied with fluence. As the photolysis energy was lowered, the leading edge decreased faster than the rest of the spectrum, indicating a multiple-photon process. As discussed below, the polarization dependence of the TOF spectra are also consistent with a multi-photon process. To obtain the threshold of the fastest hydrogen deriving from a one-photon process, the spectrum from the lowest photolysis energy should be used. Figure 6 shows a plot of signal versus  $\{h\nu - (1 + m_{\text{H}}/m_{\text{NCO}}) \cdot E_{\text{H}}\}$  for 7 mJ of photolysis energy. As per eqs 8 and 9, the extrapolated onset corresponds to the minimum  $E_{\text{int}}(\text{NCO})$ , yielding  $D_0(\text{H-NCO}) \leq 110.1 \pm 0.5 \text{ kcal mol}^{-1}$ . The uncertainty is due to (i) determining the threshold, (ii) neglecting  $E_{\text{int}}(\text{HNCO})$  and the last term in eq 5, and (iii) the photolysis laser linewidth and the resolution of the TOF spectrometer.

Here we comment further on the leading edge. If  $\text{NH}(a^1\Delta)$  absorbs a 193.3-nm photon, two spin-allowed channels are possible:  $\text{N}(^2\text{D}) + \text{H}(^2\text{S})$  and  $\text{N}(^2\text{P}) + \text{H}(^2\text{S})$ . However, an electric dipole transition from the  $a^1\Delta$  state to the repulsive  $^1\Sigma^-$  excited state [which correlates to  $\text{N}(^2\text{D}) + \text{H}(^2\text{S})$ ] is orbitally forbidden. On the other hand, a transition from  $a^1\Delta$  to the repulsive  $^1\Pi$  excited state [which correlates to  $\text{N}(^2\text{P}) + \text{H}(^2\text{S})$ ] is orbitally allowed. The energetics are shown in Figure 7.  $E_{\text{H}}$  from the

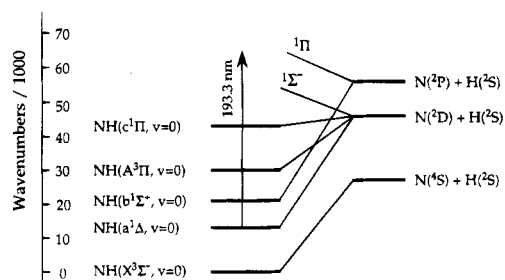


Figure 7. Energy level diagram of NH. Energies are from refs 35, 36, and 61.

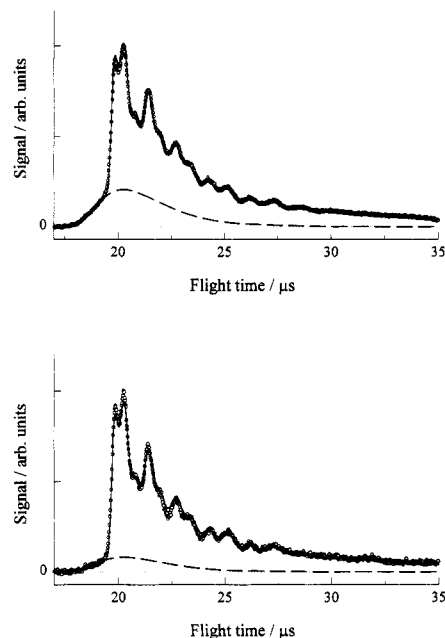
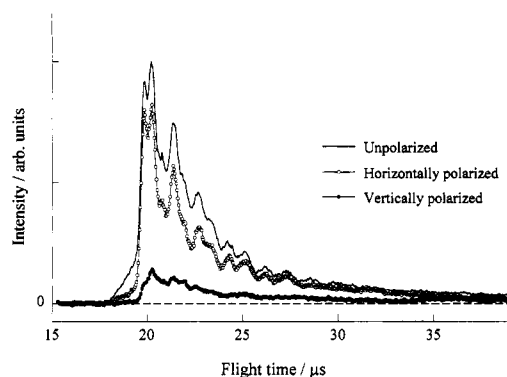


Figure 8. Simulated H atom TOF spectra with both primary and secondary dissociation processes. Circles, experimental data; solid line, total fitted spectra; long dashed line, secondary dissociation. Upper and lower traces are for 28 and 12 mJ, respectively, normalized to the photolysis laser fluences.

$\text{N}(^2\text{D}) + \text{H}(^2\text{S})$  channel is  $\sim 50 \text{ kcal mol}^{-1}$  for  $\text{NH}(a^1\Delta, v=0)$ , i.e., far larger than the leading edge, while  $E_{\text{H}}$  from  $\text{N}(^2\text{P}) + \text{H}(^2\text{S})$  is  $\sim 24 \text{ kcal mol}^{-1}$  for  $\text{NH}(a^1\Delta, v=0)$ , i.e., far smaller than the leading edge. However, nascent  $\text{NH}(a^1\Delta)$  is known to be vibrationally excited,<sup>23</sup> and  $E_{\text{H}}$  from photodissociation of  $\text{NH}(a^1\Delta, v=1,2) \rightarrow \text{N}(^2\text{P}) + \text{H}(^2\text{S})$  lies near the leading edge. Since  $\text{NH} + \text{CO}$  is the dominant primary dissociation channel and  $v = 1$  and 2 account for about 20% and 2% of the population, respectively, this is one possibility.

To illustrate this in more detail, modeling of the  $\text{NH}(a^1\Delta)$  secondary photodissociation  $\text{NH}(a^1\Delta) \rightarrow \text{N}(^2\text{P}) + \text{H}(^2\text{S})$  was carried out by using a forward-convolution program<sup>40</sup> with a slight modification. In this procedure, H atom time-of-flight spectra were calculated by using trial cm translational energy distributions of the primary H atom dissociation channel and the secondary dissociation channel convoluted with the detector and molecular beam functions. The translational energy distribution of the primary  $\text{NH} + \text{CO}$  channel used in the calculation was obtained from previous studies.<sup>17,18,21,23</sup> The calculated spectra were iteratively optimized by comparison with the experimental spectra and readjustment of the trial cm translational energy distributions. These optimized cm translational energy distributions are used to calculate TOF spectra at different laser fluences with only the laser fluence varied. The results of modeling NH secondary photodissociation are shown in Figure 8. The calculated contribution from secondary photodissociation has a general feature similar to the difference



**Figure 9.** Polarization dependence. Upper, middle, and lower traces are for unpolarized, horizontal, and vertical polarizations, respectively.

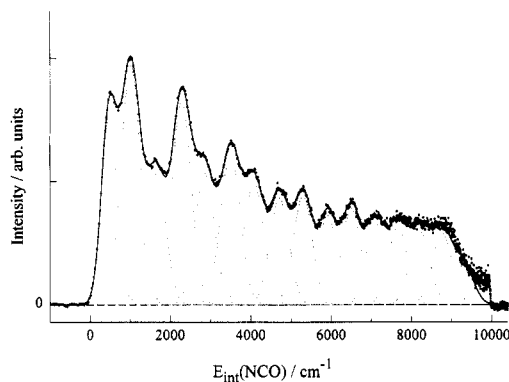


**Figure 10.** NCO internal energy distribution. See text for details.

between the experimental TOF spectra at high and lower laser fluence. This modeling suggests that  $\text{NH}(v=1)$  contributes most to the second dissociation process. Modeling of the leading edge should be reliable, despite uncertainty regarding the slow part of the second dissociation contribution.

Another possible explanation for the fast leading edge is multiple photon dissociation of clusters, since  $\text{HNCO}$  tends to polymerize.

To summarize, the cm translational energy distribution peaks near the maximum available energy with  $\langle E_{\text{cm}} \rangle \approx 0.70E_{\text{avail}}$ .

**B. NCO Internal Energy Distribution.** On average,  $E_{\text{int}}(\text{NCO})$  accounts for 30% of the available energy. The structure in the spectrum is attributed to NCO vibrations, with the internal energy distribution obtained by using

$$E_{\text{int}}(\text{NCO}) = h\nu - D_0(\text{H-NCO}) - E_{\text{cm}} \quad (10)$$

Figure 10 shows the result with the secondary photodissociation background subtracted. Though low vibrational levels are the most populous, it is clear that many excited levels are populated as well.

**C. Polarization Dependence.** Polarization dependence can provide information about electronic states involved in photodissociation. As shown in Figure 2, when  $\mathbf{E}$  lies in the plane defined by the molecular and photolysis beams and is perpendicular to the flight path, it is defined as horizontal polarization.  $\mathbf{E}$  pointing toward the detector is defined as vertical polarization. Spectra were recorded with unpolarized and horizontally and vertically polarized radiations. They are shown in Figure 9 after being normalized to the number of pulses; no correction was made for imperfect polarization. There is a significant angular anisotropy, with horizontal polarization yielding much larger signals than vertical polarization. The fragment angular distribution is given by<sup>41</sup>

$$I(\theta) \propto 1 + \beta P_2(\cos \theta) \quad (11)$$

where  $\beta$  is the asymmetry parameter,  $\theta$  is the angle between  $\mathbf{E}$  and the direction of detection, and  $P_2(\cos \theta)$  is the second Legendre polynomial. After correcting for imperfect polarization,  $\beta$  was found to be about  $-0.85 (\pm 0.1)$ , indicating a perpendicular transition.

#### IV. Discussion

**A.  $D_0(\text{H-NCO})$ .** The present results indicate  $D_0(\text{H-NCO}) \leq 110.1 \pm 0.5 \text{ kcal mol}^{-1}$ . This is less than the Okabe value of  $113.0 \text{ kcal mol}^{-1}$ .<sup>12</sup> However, the Okabe number was obtained with a room temperature sample, and therefore the upper limit in Okabe's study *after correcting for internal energy* is  $114.1 \text{ kcal mol}^{-1}$ . With the latter, the NCO ground state should be between the second and the third peak in the spectrum shown in Figure 6. Our results show that  $D_0(\text{H-NCO})$  is definitely less than  $114.1 \text{ kcal mol}^{-1}$ . Employing the same technique as Okabe, Uno and co-workers obtained an upper limit of  $111 \text{ kcal mol}^{-1}$  by using synchrotron radiation.<sup>13</sup> After correcting for the internal energy of  $\text{HNCO}$  at room temperature,  $D_0(\text{H-NCO}) \leq 112 \text{ kcal mol}^{-1}$  was obtained. Synchrotron radiation is much more intense than the radiation emanating from the hydrogen discharge lamp used in Okabe's study.<sup>12</sup> It is therefore more desirable for determining the NCO( $A^2\Sigma$ ) appearance threshold and can give a better estimation of the dissociation energy. Tokue and Ito's electron impact study gave a bond energy of  $126 \pm 14 \text{ kcal mol}^{-1}$ .<sup>24</sup> However, this experiment suffered from the low resolution of the electron energy and is less reliable than the VUV photodissociation studies. The above upper limits of  $D_0(\text{H-NCO})$  are higher than ours, though they are consistent with our value. Of the above, our results agree best with the value obtained by Uno and co-workers.<sup>13</sup>

The  $D_0(\text{H-NCO})$  value determined here is in excellent agreement with a recent experimental study by Ruscic and Berkowitz,<sup>25</sup> who used photoionization mass spectrometry to obtain  $D_0(\text{H-NCO}) \leq 110.1 \pm 0.3 \text{ kcal mol}^{-1}$  following a careful analysis of their data. Additionally, our results agree with high-level ab initio calculations, which give  $110.4 \text{ kcal mol}^{-1}$ .<sup>27,28</sup>

$D_0(\text{H-NCO})$  can be used to obtain heats of formation for NCO and  $\text{HNCO}$ . For example, the Cyr et al. value of  $\Delta H_{f,0}^0(\text{NCO}) = 30.5 \pm 1 \text{ kcal mol}^{-1}$  yields  $\Delta H_{f,0}^0(\text{HNCO}) = -28.0 \pm 1 \text{ kcal mol}^{-1}$ , in agreement with the East and Allen ab initio value of  $-27.5 \pm 0.5 \text{ kcal mol}^{-1}$ .<sup>28</sup> Alternatively, combining our result with the East and Allen value yields  $\Delta H_{f,0}^0(\text{NCO}) = 31.0 \pm 0.7 \text{ kcal mol}^{-1}$ , in agreement with Cyr et al.

Finally, we note that the discrepancy in the NCO heat of formation between the studies of Cyr et al.<sup>29</sup> and Spiglanin et al.<sup>19</sup> originates from two sources of uncertainty. One is the heat of formation of  $\text{HNCO}$ . Spiglanin et al. derived a value of  $\Delta H_{f,0}^0(\text{HNCO})$  of  $-24.9_{-2.8}^{+0.7} \text{ kcal mol}^{-1}$ , which corresponds to  $-24.2_{-2.8}^{+0.7} \text{ kcal mol}^{-1}$  at 0 K. This differs from both the ab initio value and the value derived in this study by about  $3 \text{ kcal mol}^{-1}$ . The other source of uncertainty is  $D_0(\text{H-NCO})$ , which also differs by about  $3 \text{ kcal mol}^{-1}$ . Our study lowers the value of  $D_0(\text{H-NCO})$  from that of Okabe's, thereby reducing the difference of the  $\Delta H_{f,0}^0(\text{NCO})$  value between the studies of Cyr et al. and Spiglanin et al. to about  $3 \text{ kcal mol}^{-1}$ . This brings about agreement, albeit just within the stated error limits.

**B. State and Angular Distributions and Photodissociation Mechanism.** Our data indicate a propensity toward cm translation. Namely,  $\langle E_{\text{cm}} \rangle = 70\%$  of  $E_{\text{avail}}$ , as opposed to the Yi and Bersohn value of  $30\%$ .<sup>20</sup> To obtain  $\langle E_{\text{cm}} \rangle$  from Doppler-broadened LIF spectra, they assumed an isotropic angular distribution. However, the angular distribution is *anisotropic* and this may account for the discrepancy. Note that isoelec-

tronic  $\text{HN}_3$  has been studied extensively,<sup>23,42-44</sup> and  $\langle E_{\text{cm}} \rangle$  for the H atom channel at 193.3 nm is 80% of  $E_{\text{avail}}$ ,<sup>42</sup> which is similar to our HNCO results. Such large propensities toward cm translation suggest direct dissociation via a repulsive surface. For example, in the impulsive limit, about 96% of the energy available for products is channeled into cm translation.<sup>45,46</sup>

As shown in Figure 1, only the NCO  $X^2\Pi$  electronic state is accessible.<sup>47</sup> Though the  $^2\Pi_{3/2}$  and  $^2\Pi_{1/2}$  spin-orbit states are separated by  $95.6 \text{ cm}^{-1}$ , the excimer laser linewidth of  $\sim 150 \text{ cm}^{-1}$  precludes the possibility of resolving these states. The peaks in the  $E_{\text{int}}(\text{NCO})$  distribution are separated by roughly  $600 \text{ cm}^{-1}$  and have widths of  $500\text{--}600 \text{ cm}^{-1}$ . This structure is due to vibration. The distribution peaks near the ground state with population extending to high bending levels.

Only modest rotational excitation is anticipated. Ignoring nuclear spin, angular momentum conservation requires  $\mathbf{J} = \mathbf{L} + \mathbf{j}$ , where  $\mathbf{J}$  is the total angular momentum,  $\mathbf{L}$  is the product orbital angular momentum, and  $\mathbf{j}$  is the NCO rotational angular momentum. Since  $|\mathbf{J}|$  is small, it follows that  $|\mathbf{j}| \approx |\mathbf{L}| \approx \mu b v_{\text{rel}}$ , where  $\mu$  is the reduced mass of the products,  $b$  is the exit channel impact parameter, and  $v_{\text{rel}}$  is the relative velocity of the products. Because  $\mu$  is small, NCO rotational excitation is expected to be small. Using the maximum value of  $v_{\text{rel}}$  and assuming  $b = 1.3 \text{ \AA}$  yield  $|\mathbf{j}| = 36\hbar$ , corresponding to a rotational energy of about  $500 \text{ cm}^{-1}$ .

The spectroscopy of NCO indicates several interactions: Renner-Teller, spin-orbit, and Fermi resonance.<sup>47-52</sup> Electronic transitions from  $X^2\Pi$  to the low-lying  $A^2\Sigma^+$  and  $B^2\Pi$  states were studied and analyzed in detail,<sup>47-49</sup> and the lower  $X^2\Pi$  vibronic levels are well characterized. Furthermore, term values of higher  $X^2\Pi$  vibrational levels (especially bending) were determined from (i) LIF scans of NCO produced in the  $\text{CN} + \text{O}_2$  reaction,<sup>50</sup> (ii) LIF scans of NCO in flames,<sup>51</sup> and (iii) SEP spectroscopy of NCO in a supersonic jet.<sup>52</sup> The electronic ground state was also characterized by infrared spectroscopy,<sup>53</sup> and the recommended vibrational frequencies are  $1270$ ,  $535.4$ , and  $1920.6 \text{ cm}^{-1}$ .<sup>54</sup> However, because of large Renner-Teller and spin-orbit interactions, spacings of  $X^2\Pi$  vibronic levels are complex.<sup>55</sup>

To better understand the NCO internal energy distribution, the spectrum was fitted by convoluting Gaussian functions representing vibrational levels (Figure 10); widths of  $\sim 550 \text{ cm}^{-1}$  include the excimer linewidth and the TOF spectrometer function. As noted above, modest rotational excitation is anticipated:  $\langle E_{\text{rot}} \rangle \approx 0.04 E_{\text{avail}}$ . Peak positions and relative intensities are listed in Table 2. The positions are used to label levels that can be assigned mainly to the bend vibration. Figure 11 shows a plot of peak position versus the parameter  $\nu$ . The points fit the expression  $(600 \pm 75 \text{ cm}^{-1})\nu$ , implicating the bend. However, the intensities cannot be rationalized solely on the basis of a bending progression. For example, peak 4 most likely contains a contribution from (1 1 0) and/or (0 0 1) in addition to (0 3 0). This may explain, at least in part, the intensities of peaks 4, 5, and 6. Similarly, peak 3 might be due to Fermi resonance between (1 0 0) and (0 2 0). Possible assignments are given in Table 2.

NCO vibrational excitation can be understood by comparing the geometries of the HNCO excited state and the NCO ground state (Figure 12). The first excited state of HNCO is either *cis* or *trans* with an N-C-O angle near  $120^\circ$ ,<sup>6</sup> consistent with Walsh's rule<sup>57</sup> and semiempirical molecular orbital calculations.<sup>8</sup> Since the NCO ground state is linear, bending excitation is anticipated, and our results are consistent with this. Stretching excitation is also expected. Specifically, the average of the N-C and C-O bond lengths in the HNCO excited state is near  $1.3 \text{ \AA}$ ,

TABLE 2: Parameters for the Spectrum Associated with Figure 10

peak	$\text{cm}^{-1}$ <sup>a</sup>	rel area <sup>b</sup>	possible assignment ( $\nu_1 \nu_2 \nu_3$ )
1	0	0.083	(0 0 0)
2	540	0.128	(0 1 0)
3	1170	0.070	(0 2 0), (1 0 0)
4	1810	0.107	(0 3 0), (1 1 0), (0 0 1)
5	2370	0.072	(0 4 0), (0 1 1)
6	3010	0.082	(0 5 0), (2 1 0), (1 0 1)
7	3600	0.067	(0 6 0)
8	4420	0.056	(0 7 0)
9	4810	0.057	(0 8 0)
10	5430	0.046	(0 9 0)
11	6020	0.049	(0 10 0)
12	6620	0.042	(0 11 0)
13	7180	0.041	(0 12 0)
14	7730 <sup>c</sup>	0.040	(0 13 0)
15	8280 <sup>c</sup>	0.039	(0 14 0)
16	8820 <sup>c</sup>	0.022	(0 15 0)

<sup>a</sup> Relative to peak 1; estimated uncertainty is  $\pm 75 \text{ cm}^{-1}$ . <sup>b</sup> Estimated uncertainty is  $\pm 10\%$  of the listed value. <sup>c</sup> Due to their large uncertainty, these listed values are not used in the linear fit in Figure 11.

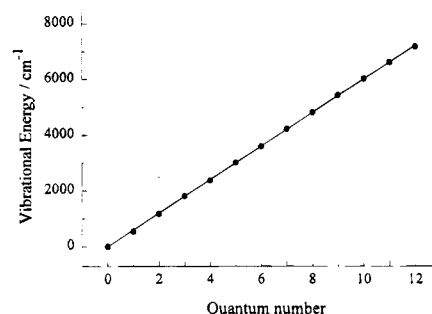


Figure 11. Vibrational energy vs quantum number.

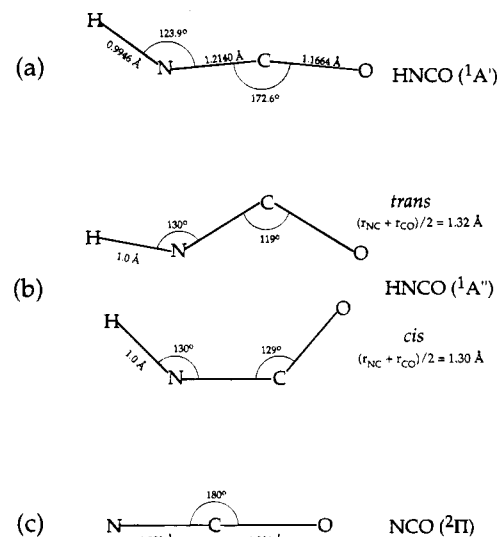


Figure 12. Geometries of ground-state  $\text{HNCO}(1^1A'')$ ,<sup>9-11</sup> excited-state  $\text{HNCO}(1^1A'')$ ,<sup>6</sup> and ground-state  $\text{NCO}(X^2\Pi)$ .<sup>56</sup>

while in the NCO ground state the N-C and C-O bond lengths are both near  $1.2 \text{ \AA}$ .

Similar excitations have been observed in the UV photodissociation of  $\text{HN}_3$  and  $\text{HNCS}$ .<sup>42,58</sup> With  $\text{HN}_3$ , the translational energy distribution of the H atom channel was measured,<sup>42</sup> and  $\text{N}_3$  was shown to be vibrationally excited. However, due to modest resolution, only the symmetric stretch was observed,<sup>42b</sup> though a large amount of bend was expected.<sup>42a</sup> The NCS internal state distribution was measured by LIF following UV photodissociation of  $\text{HNCS}$ , and the three vibrational modes were shown to be equally excited.<sup>58</sup>

The hydrogen angular distribution was obtained via polarization dependence, with **E** horizontal yielding much larger signals than **E** vertical. Clearly, the 193.3-nm transition moment lies perpendicular to the molecular plane. The  $\beta$  value of  $\sim -0.85$  is consistent with an  $1^1A''$  excited state accessed by the  $(2a'')^1(10a') \leftarrow (2a'')^2$  transition, in agreement with Dixon and Kirby<sup>6</sup> and Rabalais et al.<sup>7,8</sup> The anisotropic angular distribution also suggests that the excited-state lifetime is short, consistent with  $1^1A''$  being repulsive.

The HNCO  $2a''$  HOMO is a nonbonding out-of-plane  $\pi$  orbital with weak bonding character in the N–C region, while the  $10a'$  LUMO is in-plane with antibonding character in the N–C region and weak antibonding character in the N–H region.<sup>59</sup> As shown in Figure 1,  $1^1A''$  correlates with both  $NH(a^1\Delta) + CO(X^1\Sigma^+)$  and  $H(2S) + NCO(X^2\Pi)$ . Its energy is  $\sim 5.9$  eV and the next excited state ( $2^1A''$ ) is not likely to be reached at 193.3 nm.<sup>7,24</sup> Therefore,  $1^1A''$  is probably responsible for the two dissociation channels. To understand the dynamics better, ab initio calculations of the  $1^1A''$  PES would be helpful, as was the case for  $HN_3$ .<sup>60</sup> Namely, it was shown that  $1^1A''$  is repulsive along the  $N_2$ –NH coordinate, and in the Franck–Condon region there are pronounced gradients toward bent N–N–N. This might account for  $N_2$  rotational excitation in the  $NH + N_2$  channel<sup>43,44</sup> as well as  $N_3$  bending excitation in the  $H + N_3$  channel. On the other hand, the calculated N–N–H bending-angle dependence on the  $1^1A''$  upper surface is comparable to that on the  $1^1A'$  ground state, and because of the small H atom mass,  $N_3$  rotational excitation is modest.<sup>42</sup> The photodissociations of  $HN_3$  and HNCO yield similar product state distributions for both channels,<sup>17–23,42–44</sup> and general features of the  $1^1A''$  PES should be common to both species.

## V. Conclusion

The cm translational energy distribution in the 193.39-nm  $H + NCO$  photodissociation channel has been obtained, yielding  $D_0(H-NCO) \leq 110.1 \pm 0.5$  kcal mol<sup>-1</sup>. It is most probable that  $D_0(H-NCO) = 110.1 \pm 0.5$  kcal mol<sup>-1</sup>. The translational energy release peaks near the maximum available and accounts for about 70% of the available energy. NCO is vibrationally excited and rotational excitation is modest. An extensive bending progression was observed, suggesting a strongly bent N–C–O angle in excited HNCO. An anisotropic product angular distribution suggests a perpendicular transition and a direct process which most likely occurs on a repulsive surface.

**Acknowledgment.** We thank Y. Wen and J. Segall for valuable inputs and J. Berkowitz, B. Ruscic, and T. Sears for communicating their results prior to publication.

## References and Notes

- Perry, R. A.; Siebers, D. L. *Nature* **1986**, *324*, 657.
- Miller, J. A.; Bowman, C. T. *Int. J. Chem. Kinet.* **1991**, *23*, 289.
- Haynes, B. S. *Combust. Flame* **1977**, *28*, 113.
- Perry, R. A. *J. Chem. Phys.* **1985**, *82*, 5485.
- Miller, J. A.; Branch, M. C.; McLean, W. J.; Chandler, D. W.; Smooke, M. D.; Kee, R. J. *20th International Symposium on Combustion*, The Combustion Institute, 1984, p 673.
- Dixon, R. N.; Kirby, G. H. *Trans. Faraday Soc.* **1968**, *64*, 2002.
- Rabalais, J. W.; McDonald, J. R.; McGlynn, S. P. *J. Chem. Phys.* **1969**, *51*, 5103.
- Rabalais, J. W.; McDonald, J. R.; Scherr, V.; McGlynn, S. P. *Chem. Rev.* **1970**, *71*, 73.
- Yamada, K. *J. Mol. Spectrosc.* **1980**, *79*, 323.
- Herzberg, G.; Reid, C. *Discuss. Faraday Soc.* **1950**, *9*, 92.
- Reid, C. *J. Chem. Phys.* **1950**, *18*, 1544.
- Okabe, H. *J. Chem. Phys.* **1970**, *53*, 3507.
- Uno, K.; Hikida, T.; Hiraya, A.; Shobatake, K. *Chem. Phys. Lett.* **1990**, *166*, 475.
- Okabe, H. *Photochemistry of Small Molecules*; Wiley: New York, 1978.
- (a) Mui, J. Y. P.; Back, R. A. *Can. J. Chem.* **1963**, *41*, 826. (b) Wooley, W. D.; Back, R. A. *Can. J. Chem.* **1967**, *46*, 295.
- Bradley, J. N.; Gilbert, J. R.; Svejda, P. *Trans. Faraday Soc.* **1968**, *64*, 911.
- Drozdoski, W. S.; Baronavski, A. P.; McDonald, J. R. *Chem. Phys. Lett.* **1979**, *64*, 421.
- Fujimoto, G. T.; Umstead, M. E.; Lin, M. C. *Chem. Phys.* **1982**, *65*, 197.
- Spiglanin, T. A.; Perry, R. A.; Chandler, D. W. *J. Phys. Chem.* **1986**, *90*, 6184.
- Yi, W.; Bersohn, R. *Chem. Phys. Lett.* **1993**, *206*, 365.
- (a) Spiglanin, T. A.; Perry, R. A.; Chandler, D. W. *J. Chem. Phys.* **1987**, *87*, 1568. (b) Spiglanin, T. A.; Chandler, D. W. *J. Chem. Phys.* **1987**, *87*, 1577.
- Spiglanin, T. A.; Chandler, D. W. *Chem. Phys. Lett.* **1987**, *141*, 428.
- Bohn, B.; Stuhl, F. *J. Phys. Chem.* **1993**, *97*, 4891.
- Tokue, I.; Ito, Y. *Chem. Phys.* **1984**, *89*, 51.
- Ruscic, B.; Berkowitz, J. *J. Chem. Phys.* **1994**, *100*, 4498.
- Yokoyama, K.; Takane, S.; Fueno, T. *Bull. Chem. Soc. Jpn.* **1991**, *64*, 2230.
- East, A. L. L.; Johnson, C. S.; Allen, W. D. *J. Chem. Phys.* **1993**, *98*, 1299.
- East, A. L. L.; Allen, W. D. *J. Chem. Phys.* **1993**, *99*, 4638.
- Cyr, D. R.; Continetti, R. E.; Metz, R. B.; Osborn, D. L.; Neumark, D. M. *J. Chem. Phys.* **1993**, *97*, 4937.
- Lin, M. C.; He, Y.; Melius, C. F. *J. Phys. Chem.* **1993**, *97*, 9124.
- Schneider, L.; Meier, W.; Welge, K. H.; Ashfold, M. N. R.; Western, C. J. *J. Chem. Phys.* **1990**, *92*, 7027.
- Ashfold, M. N. R.; Lambert, I. R.; Mordaunt, D. H.; Morley, G. P.; Western, C. M. *J. Phys. Chem.* **1992**, *96*, 2938.
- (a) Segall, J.; Wen, Y.; Lavi, R.; Singer, R.; Wittig, C. *J. Phys. Chem.* **1991**, *95*, 8078. (b) Segall, J.; Wen, Y.; Singer, R.; Dulligan, M.; Wittig, C. *J. Chem. Phys.* **1993**, *99*, 6600.
- Zacharias, H.; Rottke, H.; Danon, J.; Welge, K. H. *Opt. Commun.* **1981**, *37*, 15.
- Huber, K. P.; Herzberg, G. *Molecular Spectra and Molecular Structure IV. Constants of Diatomic Molecules*; Van Nostrand: New York, 1979.
- Moore, C. E. *Atomic Energy Levels*; National Stand. Ref. Data Ser.; National Bureau of Standards: Washington, DC, 1971.
- Belson, D. J.; Strachan, A. N. *Chem. Soc. Rev.* **1982**, *11*, 41.
- Smith, S. R.; Jonassen, H. B. *J. Inorg. Nucl. Chem.* **1967**, *29*, 860.
- Linhard, M. Z. *Anorg. Allg. Chem.* **1938**, *236*, 200.
- (a) Zhao, X., Ph. D. Thesis, University of California, Berkeley, 1988. (b) Myers, J. D., Ph.D. Thesis, University of California, Berkeley, 1993.
- Zare, R. N. *Mol. Photochem.* **1972**, *4*, 1.
- (a) Gericke, K. H.; Lock, M.; Comes, F. *J. Chem. Phys. Lett.* **1991**, *186*, 427. (b) Haas, T.; Gericke, K.; Maul, C.; Comes, F. *J. Chem. Phys. Lett.* **1993**, *202*, 108.
- Chu, J.; Marcus, P.; Dagdigian, P. J. *J. Chem. Phys.* **1990**, *93*, 257.
- Rohrer, F.; Stuhl, F. *J. Chem. Phys.* **1988**, *88*, 4788.
- Busch, G. W.; Wilson, K. R. *J. Chem. Phys.* **1972**, *56*, 3626.
- Tuck, A. F. *J. Chem. Soc. Faraday Trans. II* **1977**, *73*, 689.
- (a) Dixon, R. N. *Philos. Trans. R. Soc. London A* **1960**, *252*, 165. (b) Bolman, P. S. H.; Brown, J. M.; Carrington, A.; Kopp, I.; Ramsay, D. A. *Proc. R. Soc. London A* **1975**, *343*, 17.
- Hemmerling, B.; Verloet, M. *Mol. Phys.* **1993**, *78*, 1423.
- Woodward, D. R.; Fletcher, D. A.; Brown, J. M. *Mol. Phys.* **1987**, *62*, 517.
- Patel-Misra, D.; Sauder, D. G.; Dagdigian, P. J. *J. Chem. Phys.* **1990**, *93*, 5448.
- Copeland, R. A.; Crosley, D. R. *Can. J. Phys.* **1984**, *62*, 1488.
- (a) Wu, M.; Northrup, F. J.; Sears, T. J. *J. Chem. Phys.* **1992**, *97*, 4583. (b) Wu, M.; Sears, T. J. *Mol. Phys.* (to be published).
- Milligan, D. E.; Jacox, M. E. *J. Chem. Phys.* **1967**, *47*, 5157.
- Jacox, M. E. *J. Phys. Chem. Ref. Data* **1990**, *19*, 1412.
- (a) Patel-Misra, D.; Sauder, D. G.; Dagdigian, P. J.; Crosley, D. R. *J. Chem. Phys.* **1991**, *95*, 2222.
- Misra, P.; Mathews, C. W.; Ramsay, D. A. *J. Mol. Spectrosc.* **1988**, *130*, 419.
- Walsh, A. D. *J. Chem. Soc.* **1953**, 2266.
- Northrup, F. J.; Sears, T. J. *J. Chem. Phys.* **1990**, *93*, 2337.
- Rauk, A.; Alewood, P. F. *Can. J. Chem.* **1977**, *55*, 1498.
- Meier, U.; Staemmler, V. *J. Phys. Chem.* **1991**, *95*, 6111.
- Bauschlicher, C. W., Jr.; Langhoff, S. R. *Chem. Phys. Lett.* **1987**, *135*, 76.